Surface Science 606 (2012) 464–469

Contents lists available at SciVerse ScienceDirect

Surface Science

journal homepage: www.elsevier.com/locate/susc

Preservation of the Pt(100) surface reconstruction after growth of a continuous layer of graphene

Louis Nilsson, Mie Andersen, Jacob Bjerre, Richard Balog, Bjørk Hammer, Liv Hornekær, Ivan Stensgaard *

Department of Physics and Astronomy, and Interdisciplinary Nanoscience Center, University of Aarhus, Ny Munkegade 120, 8000 Aarhus C, Denmark

ARTICLE INFO

Article history:
Received 16 September 2011
Accepted 7 November 2011
Available online 18 November 2011

Keywords:
Graphene
Pt(100)
Reconstruction
Scanning tunneling microscopy

ABSTRACT

Scanning tunneling microscopy shows that a layer of graphene can be grown on the hex-reconstructed Pt (100) surface and that the reconstruction is preserved after growth. A continuous sheet of graphene can be grown across domain boundaries and step edges without loss of periodicity or change in direction. Density functional theory calculations on a simple model system support the observation that the graphene can have different rotation angles relative to the hex-reconstructed Pt surface. The graphene sheet direction can be changed by incorporating pentagon-heptagon defects giving rise to accommodation of edge dislocations. The defect formation energy and the induced buckling of the graphene have been characterized by DFT calculations.

1. Introduction

Graphene, a single atomic sheet of graphite, exhibits unique electronic, mechanical and thermal properties, which could be utilized in emerging areas such as graphene-based electronic devices [1,2]. Most important for the electronic device fabrication is the high mobility of the charge carriers that behave like massless Dirac fermions [3]. However, the production of high quality, large scale graphene by cost efficient routes needs further improvements [4-8].

The synthesis of graphene is currently pursued along two different, major directions [9,10]. Micromechanical or solvent based exfoliation of graphite (a top-down technique) may lead to isolated platelets of high-quality graphene, but the dimensions are typically limited to tens or hundreds of micrometers. The seminal paper igniting renewed interest in the properties of graphene was based on experiments performed on mechanically exfoliated graphene [11]. Epitaxial growth of graphene (a bottom-up technique) can be achieved along various routes. High temperature treatment of SiC wafers leads to thermal decomposition and the formation of a graphene surface layer [12]. By exposing appropriate metal crystals or metal foils to hydrocarbons at elevated temperature, large-area graphene can be formed by chemical vapour deposition (CVD). Segregation of carbon from the bulk may also play a significant role in the growth or perfection of epitaxial graphene on some metal surfaces. Growth of graphene (and graphite) on Pt single crystal surfaces by CVD and segregation was reported more than 40 years ago [13], and CVD growth has been achieved on many different metals which catalyze dehydrogenation of hydrocarbons [14]. Recently even large scale growth of graphene on foils of Cu, a fairly non-reactive metal for dehydrogenation reactions, was reported [7,8].

The quality of the graphene produced on many metals by CVD is in general inferior to that of exfoliated graphene. The challenge is therefore to optimize the growth conditions in order to increase the domain size and reduce the number of defects. It is additionally of great importance to understand both the nature of the defects and how these defects will influence the properties of the graphene sheet. Furthermore, if the graphene should be transferred to an insulating substrate by a lift-off process, it is essential that the graphene can be grown continuously across defects such as steps and domain boundaries. Based on STM experiments on Ir(111) [15], and LEEM investigations on Ru(0001) [16] and Pt(111) [17] it has previously been demonstrated that a graphene monolayer can be grown fully coherently over step edges. Whether this is a general property of graphene growth on reactive surfaces remains to be seen.

In general graphene forms incommensurate or long-wave coincidence structures on single crystal metal surfaces, and there is a large variability in the interaction with the underlying substrate [14]. On Pt (111) more than 20 Moiré superstructures have been observed [18]. Here, we report results for Pt(100) which is known to exhibit a quasi-hexagonal surface reconstruction [19]. To our knowledge, there have been no previous detailed structural investigations of graphene formation on *reconstructed* metal surfaces. Exposure of the reconstructed Pt (100) surface to a large variety of gases such as NO, CO, O_2 and C_2H_4 leads to a lifting of the reconstruction [20-22]. Given the propensity of the reconstructed Pt(100) surface to revert to an unreconstructed state in the presence of an adsorbed layer, it is *a priori* in no way obvious that the reconstruction might survive the formation of a graphene layer on Pt(100).

* Corresponding author.
E-mail address: fysis@phys.au.dk (I. Stensgaard).

0039-6028/$ – see front matter © 2011 Elsevier B.V. All rights reserved.
doi:10.1016/j.susc.2011.11.007

Graphite formation on Pt(100) by exposure to ethylene (C_2H_4) at elevated temperatures has been addressed before, but with conflicting results. In one study [23] it was assumed that exposure of Pt(100) at elevated temperatures of 900–1300 K led to the formation of graphitic islands on an unreconstructed surface, but no microscopic technique for surface characterization was available. A LEED study [24] led to the conclusion that graphite forms during exposure to ethylene at temperatures >400 °C, but that faceting takes place at temperatures above 500 °C. An STM study [22] concluded that for exposure at RT and subsequent heating, the adsorbates appeared to desorb completely when heated above 900 K.

Here we demonstrate that a graphene sheet can be grown continuously on the Pt(100) surface *without lifting the reconstruction*, even across step edges and domain boundaries in the platinum substrate. For substrate domains which are perpendicular to each other, the graphene sheet is shown to grow across the domain boundary without defects. For domains in the substrate which are rotated ≈97° from each other, the graphene is observed to incorporate edge dislocations consistent with the presence of pentagon-heptagon defects in the boundary region to facilitate rotation of the graphene sheet.

2. Methods

2.1. Experimental

STM measurements were performed at RT in two different UHV systems using the so-called Aarhus STM [25]. The Pt (100) surface was cleaned by numerous cycles of 2 keV Ne sputtering and annealing up to 1000 °C, combined with annealing in O_2 at 700 °C, followed by flashes to 900 °C. The cleanliness of the surface was checked with STM. There is no standard procedure for synthesis of graphene on Pt. Widely different recipes for Pt(111) include exposure of a carbon-rich substrate to ethylene at 1000 °C followed by a slow lowering of temperature [17], deposition of C_{60} at room temperature followed by annealing to 930 K by electron bombardment [18], and exposure at a fixed substrate temperature between 500 °C and 800 °C [26]. In the experiments reported here, graphene growth was typically carried out by exposing the Pt surface to 100–200 L of either ethylene or propylene (C_3H_6) at pressures in the low 10^{-7} Torr range and a sample temperature of 700 °C, with periodic flashes to 900 °C. No systematic difference between exposure to ethylene and propylene was observed. The periodic flashes during growth were observed to improve the quality of the graphene film in terms of fewer defects. The detailed reason is unknown, but one might speculate that an additional mobility is imparted on the C atoms via a dissolution-segregation mechanism.

2.2. Calculations

Density functional theory (DFT) calculations were performed for two systems. The calculations regarding rotated sheets of graphene on a Pt(111) surface were performed with the semi-local meta-GGA density functional M06-L [27] implemented in the real-space projector augmented wave GPAW code [28]. This functional has proven successful in describing weak dispersive interactions such as those encountered between the sheets of graphene in graphite [29]. The supercells all contain a slab of 4 layers of Pt atoms with a graphene sheet adsorbed on one side and a vacuum region of ≈7.5 Å on each side of the slab normal to the surface. 2D Periodic boundary conditions were employed for the directions parallel to the surface. The in-plane lattice constant of graphene was fixed to its optimized value of 2.451 Å, and the Pt lattice constant was adapted accordingly. The mismatch with the optimized Pt lattice constant is in the range 0.03%-2.2% for the different supercells - a reasonable approximation. A (4,4), (4,4) and (2,2) k-point grid was used for sampling the small, medium and large supercells, respectively. The grid spacing was ≈0.16 Å. For the calculations regarding different rotations of the graphene sheet all atoms were fully relaxed, whereas for the calculations regarding the potential energy curve all atoms were kept fixed at the optimized positions for the equilibrium separation varying only the graphene-Pt separation.

The calculations regarding edge dislocation lines in graphene involved supercells with hundreds of atoms and were therefore (for reasons of computational efficiency) performed on a free-standing graphene layer with the Siesta code [30,31]. Exchange and correlation effects were described using the GGA functional of Perdew, Burke and Ernzerhof (PBE) [32]. The numerical atomic orbital basis set quality was double-ζ plus polarization orbitals and the range of the orbitals was defined through an orbital energy shift of 0.01 Ry. A mesh cutoff value of 300 Ry was used for the plane waves in the real space grid. The effects of the core electrons were described using norm-conserving pseudopotentials of the improved Trouiller-Martins type [33]. A (4,2) and (2,2) k-point grid was used for sampling the small and large supercells, respectively. 3D Periodic boundary conditions were employed, and a vacuum layer of 15 Å in the direction normal to the surface separated adjacent slabs. All atomic positions and the supercell dimensions were fully relaxed.

3. Results and discussion

An STM image of the clean platinum surface is depicted in Fig. 1(a). The clean Pt(100) surface may exhibit two different, but very similar reconstructions, depending on the preparation temperature. A conceptually simple approximant for these structures is a hexagonal Pt (111) layer, which is isotropically contracted by 3.8% and has a close-packed row either aligned with (the hex phase) or rotated by 0.7° (the hex-R0.7° phase) relative to a close-packed row in the underlying, unreconstructed Pt(100) surface [19,21]. Both reconstructions give rise to a characteristic “stripe” structure, as seen in Fig. 1(a). The surface covered by a graphene sheet also displays a stripe structure, as seen in Fig. 1(b), and the characteristic honeycomb structure is observed in the high resolution STM image, Fig. 1 (b) insert. From atomically resolved STM images such as Fig. 1(c) of a clean, reconstructed terrace (left) coexisting with a graphene covered terrace (right) we conclude that to within the experimental precision (1–2%), the graphene lattice constant is unchanged from its native value of 2.46 Å. Furthermore, the stripe superstructure observed on the right terrace in Fig. 1(c), which is graphene covered, exhibits the same periodicity and orientation as the one observed at the left terrace, which is a clean, reconstructed platinum surface. *We therefore assign the superstructure observed for graphene on Pt(100) to the platinum reconstruction structure, i.e., the graphene overlayer resides on top of the reconstructed Pt(100) surface*.

Analysis of the orientation of the graphene sheet relative to the underlying, reconstructed substrate reveals that although either an armchair or a zigzag direction of the graphene tends to be aligned or have a small angle with the direction of the superstructure stripes, other angles are possible. Armchair directions are observed at ≈5° and ≈10° with the stripe direction in Fig. 1(b) and (c), respectively, while in Fig. 3(a), a zigzag direction coincides with the stripe direction in the upper left part of the image, but becomes approximately perpendicular to the stripe direction in the lower right part of the image. These observations suggest that the interaction energy between the graphene and the reconstructed substrate does not depend strongly on the relative rotation between the graphene layer and the underlying substrate.

DFT calculations corroborate this observation. The simplest approximation to the physical system of graphene on the reconstructed Pt (100) surface is graphene on a Pt(111) surface. Fig. 2(a), (b) and (c) show models of a graphene layer with three different orientations relative to an underlying Pt(111) layer. In (a) the graphene armchair direction is aligned with the close-packed Pt direction, while in (b) and (c) the graphene layer has been rotated by 10.8° and 16.1°, respectively.

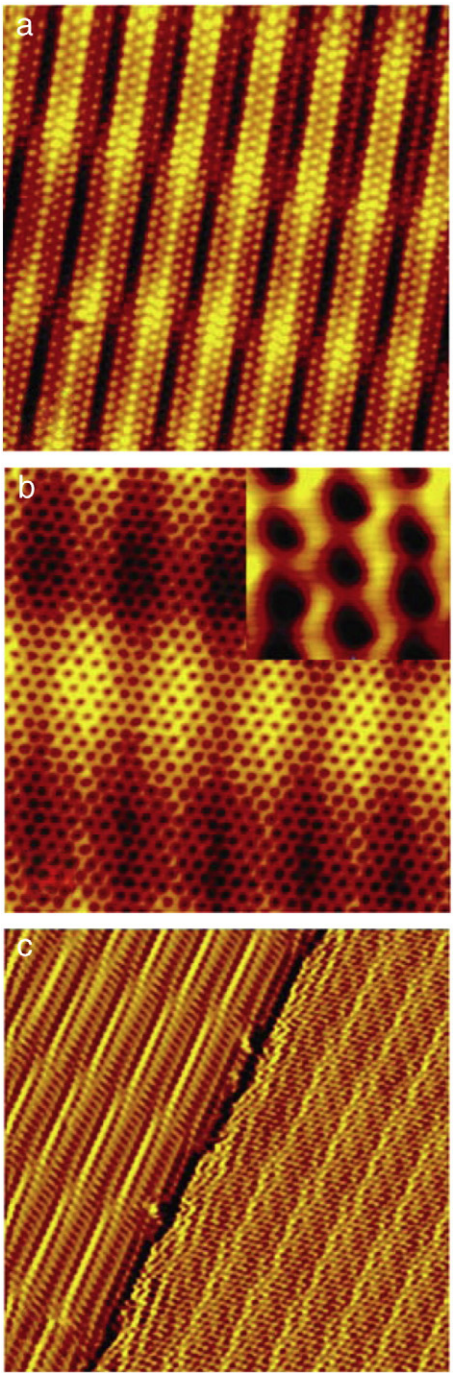

Fig. 1. (a) STM image (w × h = 110 Å × 100 Å) of the hex-R0.7° reconstructed, clean Pt(100) surface. (b) STM image (70 Å × 70 Å) of graphene grown on a hex-reconstructed Pt(100) surface. (The scan direction differs slightly from that in (a)). The inset (6 Å × 7 Å) shows the characteristic honeycomb structure of graphene. (c) STM image (140 Å × 150 Å) of two adjacent terraces separated by a step. The left (upper) terrace displays the hex-R0.7° reconstructed, clean Pt(100) surface, while the right (lower) terrace is covered with graphene. The image has been differentiated to enhance the superstructures on the terraces.

The binding energies per C atom for the three configurations are found to be 60.0 meV, 60.1 meV and 59.8 meV, respectively — very moderate differences. For the unit cell in (a) several translations of the graphene sheet away from the high symmetry adsorption sites were investigated producing only negligible changes in the binding energy. Thus we find that neither a rotation nor a translation of the graphene sheet with respect to the Pt(111) surface alters the graphene-Pt interaction. This is in good qualitative agreement with previous observations made for graphene on Pt(111). In one study [17], a large number of rotational variants was observed experimentally, suggesting a weak substrate coupling. This was confirmed by maps of the band structure, which strongly resembled that of isolated graphene. In another study of the structural properties of graphene on Pt(111) [26] the binding energies were calculated for two different graphene orientations rotated by 30° from each other with the LDA exchange-correlation functional as implemented in the VASP code. The binding energies obtained differed substantially from this work, being only around 39 meV per C atom. However, the difference in binding energy between the two rotations was only ≈1 meV, in good agreement with this work. We note that since the meta-GGA functional, M06-L has been fit using π-bonded molecules (benzene dimers) in the training database, our use of this functional for the present system which has Pt-graphene π-interactions, may be expected to provide more accurate binding energies than calculations using the very simple LDA functional. We believe that the meV/C-atom order of magnitude of the energy difference found in the two studies will be characteristic for the real system as well. (It would be attractive to calculate the binding energy for a better structural approximant to the real system, but such models will in general correspond to significant increases in the size of the unit cell).

The observed presence of the Pt reconstruction after graphene formation is in good agreement with the calculated small interaction energy between the carbon atoms in the graphene layer and the hex-reconstructed surface.

On the reconstructed surface the graphene layer exhibits a periodic, wavy structure as shown in Fig. 1(b). Due to the fact that the interaction energy between the graphene and the substrate is very small and close to independent of translation and rotation of the graphene relative to the substrate, we do not expect the spatial modulation of the graphene to be coupled to any significant periodic strain in the graphene layer. We cannot detect any strain in the STM images, and due to the computational limitations mentioned above, the DFT calculations cannot shed any light on this subject. Any strain revealed by calculations on a height modulated substrate with too small a unit cell might be an artefact resulting from the imposed coincidence structure.

The graphene layer exhibits a remarkable ability to grow uninterrupted across various obstacles. In Fig. 3(a) the graphene sheet has grown across a domain boundary between two perpendicular, reconstructed domains with no loss of periodicity or direction. An area with a step edge in the underlying platinum surface is depicted in Fig. 3(b). The zigzag direction of the graphene perpendicular to the step is seen to continue directly across the step, while the two other zigzag directions experience a lateral shift as expected from the height difference of the two terraces. A line scan perpendicular to the step along the direction indicated in Fig. 3(b) is displayed in Fig. 3(c). The regular modulation of height confirms the continuity across the step without any observable defects. We speculate that the deeper corrugation observed at the transition from the upper terrace to the sloped region is due to a decrease in DOS at the Fermi level, brought about by the increased distance to the underlying Pt atoms. The structural coherence of graphene across steps has been observed previously on Ir(111) [15], Ru(0001) [16], and Pt(111) [17], as well as on polycrystalline copper [34].

The Pt(100) hex-R0.7° reconstruction gives rise to two domains with an angular spacing of ≈8° between the stripe directions (as well as their counterparts rotated 90° by symmetry) [21]. This finding supports the observation in Fig. 4(a) of a boundary between two graphene domains with a ≈97° angle between the underlying Pt-reconstruction stripe directions.[1] A few nanometres away from the boundary the graphene sheet is orientated with an armchair direction along the platinum reconstruction in the left domain, while in the right domain, the armchair direction becomes perpendicular to the reconstruction stripes. The graphene sheet is again observed to

[1] The ≈1° deviation from the expected ≈98° angle may be due to a slight misalignment between the graphene armchair direction and the direction perpendicular to the reconstruction stripes in the right domain.

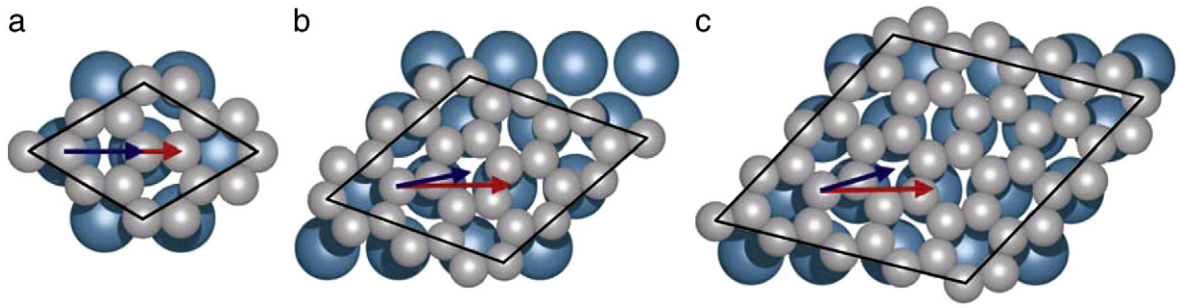

Fig. 2. (Color online) Pt atoms are shown in light blue and C atoms in grey, the Pt close-packed and graphene armchair directions are indicated with red and dark blue arrows, respectively. Structure of graphene on Pt(111) having the graphene armchair direction (a) aligned with the Pt(111) close-packed direction, (b) rotated 10.8° with respect to the Pt(111) close-packed direction and (c) rotated 16.1° with respect to the Pt(111) close-packed direction. The unit cells are indicated in black. The smaller cell contains 8 °C atoms and 3 Pt atoms per layer, the medium cell contains 18 °C atoms and 7 Pt atoms per layer and the large cell contains 32 °C atoms and 13 Pt atoms per layer.

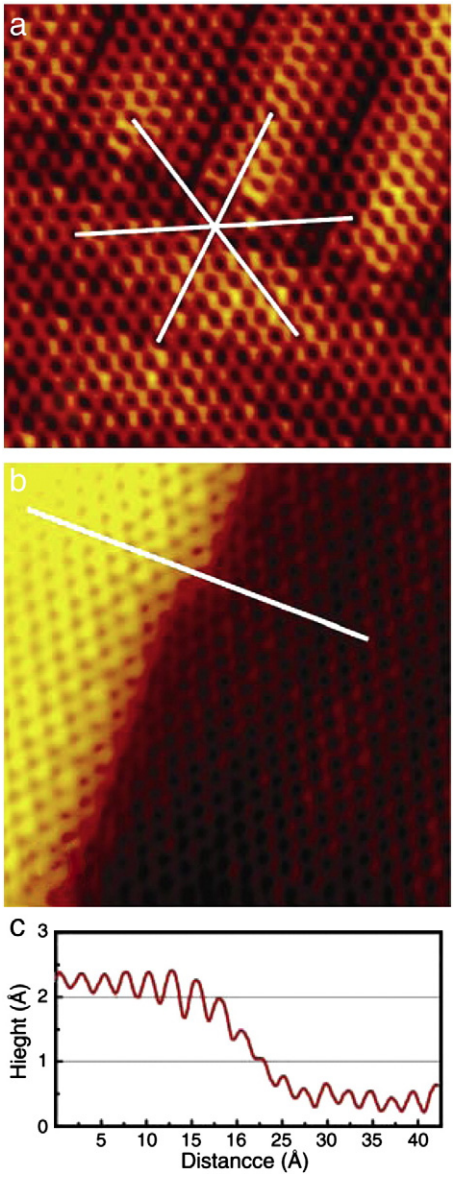

Fig. 3. (a) STM image (47 Å × 50 Å) of a graphene area with a domain boundary between two perpendicular domains of the underlying hex-reconstructed Pt(100) surface. The white lines indicate zigzag directions in the graphene. (b) STM image (47 Å × 50 Å) of a graphene area with a step in the underlying hex-reconstructed Pt (100) surface. (c) Height profile along the line shown in (b), indicating a continuous transition across the step.

grow continuously across the boundary, however, this time defects are observed in the transition region. (It should be noted that this type of defect complex was observed primarily in the beginning of this project with insufficient exposure and/or insufficient temperatures to produce a more perfect graphene layer. Since the aim of this study has been to characterize and understand the response of the graphene layer to this type of defect rather than to carry out a statistical analysis of the occurrence of the defect as a function of preparation procedure, such an analysis was not undertaken. The defect complex is suppressed on high-quality graphene films on Pt(100)).

A thorough analysis of the experimentally observed data obtained near this boundary reveals that the measured $\approx 7^{\circ}$ change in angle is mediated by the incorporation of a series of edge dislocations, i.e. by periodic incorporation along the phase boundary of an extra row of carbon rings. The upper/lower polygon depicted in Fig. 4(a) has its long sides coinciding with a zigzag/armchair direction in the two domains, while the short sides coincide with armchair/zigzag directions. The upper, short side of the topmost polygon crosses four more rows of carbon rings than the lower, short side of the polygon, corresponding to an insertion of four rows of carbon rings along the zigzag direction and a Burgers vector as indicated with a black arrow. In the lower polygon two rows of carbon rings have been inserted along the armchair direction, corresponding to the indicated Burgers vector.

Edge dislocations are common defects in graphene, where they frequently separate domains of different orientations [15,35]. The role of a dislocation core is played by a pentagon-heptagon pair reminiscent of a Stone-Wales (SW) defect [36]. SW defects can be created by a 90° in-plane rotation of two carbon atoms around the midpoint of their bond. In a hexagonal lattice this transformation leads to the creation of two pentagons and two heptagons with no change in the adjacent graphene directions. To induce a change in direction, the incorporation of only a single pair of pentagon-heptagons is considered [37].

DFT calculations have been carried out on free-standing graphene to model the two types of edge dislocations. The supercell used for modelling the defect line in the graphene armchair direction is shown in Fig. 4(b). To achieve a rotation of 7.4° (which is close to the experimentally observed $\approx 7^{\circ}$) between adjacent graphene sheets, defects consisting of a pentagon and a heptagon are incorporated with a spacing of 19.5 Å (the L_x value). For symmetry reasons the cell contains an upper and a lower defect line running in opposite directions as indicated with the black lines. An L_y value of around 37 Å was sufficient to avoid interactions between the two defect lines. The same principles were applied for constructing the supercell used for modelling the defect line in the graphene zigzag direction. The insert in Fig. 4(c) shows a side view of the cell. It is seen that the graphene layer buckles out of the plane as a consequence of the insertion of a row of carbon rings via a pentagon–heptagon pair. Thus, the buckling can be explained as a relief mechanism of the stress associated with compressing the C–C interatomic distances. Fig. 4(d) shows a close-

up of the STM image in Fig. 4(a) with the structures obtained from DFT calculations superimposed. In spite of the fact that the contrast in the STM image does not allow for observing the pentagons and heptagons directly, it is clearly seen that the proposed models are in accordance with the STM data.

The formation energy for the two types of dislocation lines was calculated as the difference between total energies of the cell with defects and a cell with the corresponding number of carbon atoms situated in a perfect graphene sheet, normalized to unit length of defect line and divided by 2 to account for having 2 defect lines per cell. The results are 0.280 eV/Å and 0.321 eV/Å for armchair and zigzag directions, respectively. The formation energies for one of the defect lines is directly comparable to previous results of [37] and overall the values are in good agreement.

For the free-standing graphene we calculate a buckling of 2.73 Å and 3.20 Å for armchair and zigzag directions, respectively. If the Pt-supported graphene were to maintain this buckling, a loss in dispersive Pt-graphene bonding must result, relative to the bonding of flat graphene. In order to estimate this energy loss we have calculated the average potential energy per carbon atom as a function of the Pt-graphene separation for the system in Fig. 2(a). The curve is shown in Fig. 4(c) along with a buckled graphene sheet (drawn to a scale consistent with the x-axis) containing a defect line in the graphene armchair direction. The loss in binding energy is now calculated for each C atom according to its height above the surface and the sum is normalized to the length of the unit cell. Optimizing the separation of the buckled graphene sheet from the surface gives a least possible energy loss of 0.125 eV/Å and 0.182 eV/Å for armchair and zigzag directions, respectively. These numbers should be compared to the difference between formation energies for cells where all atoms are constrained to a plane and cells where the graphene is allowed to buckle, which we have calculated to 0.097 eV/Å and 0.113 eV/Å for armchair and zigzag directions, respectively. For both defect line directions the loss in binding energy due to the defect induced buckling exceeds the energy cost of keeping the sheet flat. This does not necessarily mean that the graphene sheet would prefer a totally flat geometry, but that a considerable lower buckling would be expected for the case of graphene adsorbed on the substrate. Indeed, from the STM images we estimate a buckling of only ≈1.2 Å. A buckling of this magnitude fits in nicely with the width of the potential energy well in Fig. 4(c), thus avoiding having carbon atoms with excessive increases in potential energy. Due to the approximate nature of this method, we cannot calculate the precise value of the optimum buckling of the graphene caused by the incorporation of the edge dislocation.

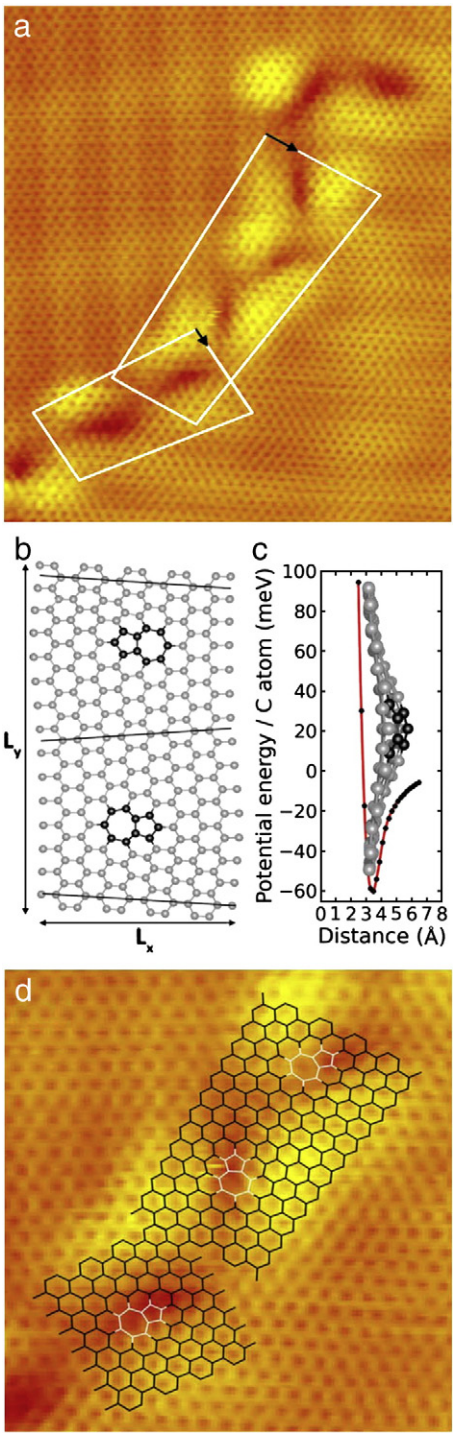

Fig. 4. (a) STM image (100 Å × 130 Å) of the graphene sheet in a region encompassing the domain boundary between two hex-reconstructed Pt domains having an angle of ≈97°. Two different types of edge dislocation lines are seen. In the lower left part of the image the line runs along the graphene armchair direction and consists of regular spaced defects of the same kind, whereas in the middle part of the image the line runs along the graphene zigzag direction and alternates between two different orientations of defects. Polygons in white are drawn around two defects in the lower defect line and two pairs of defects in the upper defect line. The black arrows indicate Burgers vectors and span two graphene zigzag unit vectors and two graphene armchair unit vectors, respectively, for the lower and upper polygon. (b) Structure of the supercell used for DFT calculations on the lower defect line. For symmetry reasons it contains an upper and a lower defect line running in opposite directions as indicated with the black lines. The C atoms involved in topological defects, i.e. C atoms in pentagons and heptagons, are shown in black. (c) Potential energy curve for the graphene on Pt(111) system in Fig. 2(a). The black dots are calculated values and the red line is a cubic spline interpolation. The insert shows a side view of the lower half of (b) at its minimum energy position in the potential energy curve. (d) Close-up (52 Å × 58 Å) of the STM image in (a) at the position where the two types of defect lines meet, with structures from DFT calculations on the two defect lines superimposed. C atoms in pentagons and heptagons are shown in white.

4. Conclusion

In conclusion we have shown by STM measurements that exposure of the hex-reconstructed Pt(100) surface to ethylene or propylene at elevated temperature leads to the formation of a graphene layer *residing on top of the reconstructed surface*. A continuous sheet of graphene can be grown across domain boundaries and step edges. Different rotation angles of the graphene relative to the hex-reconstructed Pt surface have been observed, suggesting that the rotation energy of the graphene relative to the substrate is small. DFT calculations on a simple model system support this assumption. To change from zigzag to armchair (or vice versa) alignment with the underlying Pt reconstruction superstructure across a boundary between two domains which are rotated by ≈97° from each other, the graphene sheet can incorporate edge dislocations. DFT calculations show that the incorporation of pentagon-heptagon

pairs as a "source" of edge dislocations may lead to an angular shift of the observed magnitude as well as a buckling of the graphene layer, consistent with the experimental observations.

The ability to grow continuous graphene sheets on a reconstructed surface opens up new opportunities for spatial modulation of graphene sheets residing on substrates. The observed high structural quality across substrate boundaries is important for large-scale production of graphene and vital for real applications of the graphene as a template for surface science applications or, via lift-off techniques, in e.g. electronic components.

References

[1] A.K. Geim, K.S. Novoselov, Nat. Mater. 6 (2007) 183.
[2] J. Hass, R. Feng, T. Li, X. Li, Z. Zong, W.A. de Heer, P.N. First, E.H. Conrad, C.A. Jeffrey, C. Berger, Appl. Phys. Lett. 89 (2006) 143106.
[3] K.S. Novoselov, A.K. Geim, S.V. Morozov, D. Jiang, M.I. Katsnelson, I.V. Grigorieva, S.V. Dubonos, A.A. Firsov, Nature 438 (2005) 197.
[4] K.V. Emtsev, A. Bostwick, K. Horn, J. Jobst, G.L. Kellogg, L. Ley, J.L. McChesney, T. Ohta, S.A. Reshanov, J. Rohrl, E. Rotenberg, A.K. Schmid, D. Waldmann, H.B. Weber, T. Seyller, Nat. Mater. 8 (2009) 203.
[5] K.S. Kim, Y. Zhao, H. Jang, S.Y. Lee, J.M. Kim, J.H. Ahn, P. Kim, J.Y. Choi, B.H. Hong, Nature 457 (2009) 706.
[6] A. Reina, X.T. Jia, J. Ho, D. Nezich, H.B. Son, V. Bulovic, M.S. Dresselhaus, J. Kong, Nano Lett. 9 (2009) 30.
[7] L. Colombo, X.S. Li, W.W. Cai, J.H. An, S. Kim, J. Nah, D.X. Yang, R. Piner, A. Velamakanni, I. Jung, E. Tutuc, S.K. Banerjee, R.S. Ruoff, Science 324 (2009) 1312.
[8] S. Bae, H. Kim, Y. Lee, X.F. Xu, J.S. Park, Y. Zheng, J. Balakrishnan, T. Lei, H.R. Kim, Y.I. Song, Y.J. Kim, K.S. Kim, B. Ozyilmaz, J.H. Ahn, B.H. Hong, S. Iijima, Nat. Nanotechnol. 5 (2010) 574.
[9] Y.W. Zhu, S. Murali, W.W. Cai, X.S. Li, J.W. Suk, J.R. Potts, R.S. Ruoff, Adv. Mater. 22 (2010) 3906–3924.
[10] L. Zhai, V. Singh, D. Joung, S. Das, S.I. Khondaker, S. Seal, Prog. Mater. Sci. 56 (2011) 1178.
[11] K.S. Novoselov, A.K. Geim, S.V. Morozov, D. Jiang, Y. Zhang, S.V. Dubonos, I.V. Grigorieva, A.A. Firsov, Science 306 (2004) 666.
[12] C. Berger, Z.M. Song, X.B. Li, X.S. Wu, N. Brown, C. Naud, D. Mayou, T.B. Li, J. Hass, A.N. Marchenkov, E.H. Conrad, P.N. First, W.A. de Heer, Science 312 (2006) 1191.
[13] J.W. May, Surf. Sci. 17 (1969) 267.
[14] J. Wintterlin, M.L. Bocquet, Surf. Sci. 603 (2009) 1841.
[15] J. Coraux, A.T. N'Diaye, C. Busse, T. Michely, Nano Lett. 8 (2008) 565.
[16] P.W. Sutter, J.I. Flege, E.A. Sutter, Nat. Mater. 7 (2008) 406.
[17] P. Sutter, J.T. Sadowski, E. Sutter, Phys. Rev. B 80 (2009).
[18] J.A. Martin-Gago, P. Merino, M. Svec, A.L. Pinardi, G. Otero, Acs Nano 5 (2011) 5627.
[19] P. Heilmann, K. Heinz, K. Muller, Surf. Sci. 83 (1979) 487.
[20] P. Gardner, M. Tushaus, R. Martin, A.M. Bradshaw, Surf. Sci. 240 (1990) 112.
[21] A. Borg, A.M. Hilmen, E. Bergene, Surf. Sci. 306 (1994) 10.
[22] M. Ronning, E. Bergene, A. Borg, S. Ausen, A. Holmen, Surf. Sci. 477 (2001) 191.
[23] T. Zecho, A. Horn, J. Biener, J. Kuppers, Surf. Sci. 397 (1998) 108.
[24] B. Lang, Surf. Sci. 53 (1975) 317.
[25] E. Laegsgaard, F. Besenbacher, K. Mortensen, I. Stensgaard, J. Microsc. (Oxford) 152 (1988) 663.
[26] M. Gao, Y. Pan, L. Huang, H. Hu, L.Z. Zhang, H.M. Guo, S.X. Du, H.J. Gao, Appl. Phys. Lett. 98 (2011) 033101.
[27] Y. Zhao, D.G. Truhlar, J. Chem. Phys. 125 (2006) 194101.
[28] J. Enkovaara, C. Rostgaard, J.J. Mortensen, J. Chen, M. Dulak, L. Ferrighi, J. Gavnholt, C. Glinsvad, V. Haikola, H.A. Hansen, H.H. Kristoffersen, M. Kuisma, A.H. Larsen, L. Lehtovaara, M. Ljungberg, O. Lopez-Acevedo, P.G. Moses, J. Ojanen, T. Olsen, V. Petzold, N.A. Romero, J. Stausholm-Moller, M. Strange, G.A. Tritsaris, M. Vanin, M. Walter, B. Hammer, H. Hakkinen, G.K.H. Madsen, R.M. Nieminen, J. Norskov, M. Puska, T.T. Rantala, J. Schiotz, K.S. Thygesen, K.W. Jacobsen, J. Phys. Condens. Matter 22 (2010) 253202.
[29] G.K.H. Madsen, L. Ferrighi, B. Hammer, J. Phys. Chem. Lett. 1 (2010) 515.
[30] J.M. Soler, E. Artacho, J.D. Gale, A. Garcia, J. Junquera, P. Ordejon, D. Sanchez-Portal, J. Phys. Condens. Matter 14 (2002) 2745.
[31] E. Artacho, E. Anglada, O. Dieguez, J.D. Gale, A. Garcia, J. Junquera, R.M. Martin, P. Ordejon, J.M. Pruneda, D. Sanchez-Portal, J.M. Soler, J. Phys. Condens. Matter 20 (2008) 064208.
[32] J.P. Perdew, K. Burke, M. Ernzerhof, Phys. Rev. Lett. 77 (1996) 3865.
[33] N. Troullier, J.L. Martins, Phys. Rev. B 43 (1991) 1993.
[34] H.I. Rasool, E.B. Song, M.J. Allen, J.K. Wassei, R.B. Kaner, K.L. Wang, B.H. Weiller, J.K. Gimzewski, Nano Lett. 11 (2011) 251.
[35] F. Banhart, J. Kotakoski, A.V. Krasheninnikov, Acs Nano 5 (2010) 26.
[36] A.J. Stone, D.J. Wales, Chem. Phys. Lett. 128 (1986) 501.
[37] O.V. Yazyev, S.G. Louie, Phys. Rev. B 81 (2010) 195420.